CHEMICAL INTERACTIONS OF THE $Ba_2YCu_3O_{6+x}$ SUPERCONDUCTOR WITH COATED CONDUCTOR BUFFER LAYERS

[1]W. Wong-Ng, [1]Z. Yang, [1]G. Liu, [1]Q. Huang, [1]L.P. Cook, [1]S. Diwanji, [1]C. Lucas, [2]M-H. Jang, and [3]J.A. Kaduk
[1]NIST, Gaithersburg, MD 20899.
[2]Yonsei University, Seoul, Republic of Korea, 120-740.
[3]Illinois Institute of Technology, Chicago IL 60616

ABSTRACT

Reactions between the high T_c superconductor $Ba_2YCu_3O_{6+x}$ and the potential buffer layer materials $SrTiO_3$, Gd_3NbO_7, $LaMnO_3$, and CeO_2 have been investigated using x-ray powder diffraction and other analytical techniques. Reaction products include $(Ba,Sr)_3YTi_2O_x$, $(Ba,Sr)_2YCu_3O_{6+x}$, $(Sr,Br)TiO_3$, $(Sr,Ba)_2TiO_4$, CuO_x, $(Gd_xY_{3-x})NbO_7$, $(Y,Gd)_2Cu_2O_5$, $Ba_2(Gd_xY_{1-x})NbO_6$, $(Gd,Y)_2CuO_4$, $Ba_2(Gd_xY_{1-x})Cu_3O_{7-x}$, $Ba_{2-x}(La_{1+x-y}Y_y)Cu_3O_{6+z}$, $Ba(Y,La)_2CuO_5$, $(La,Y)MnO_3$, $(La,Y)Mn_2O_5$, and $Ba(Ce,Y)O_{3-x}$, and most of these have been characterized structurally. The reaction of $Ba_2YCu_3O_{6+x}$ and CeO_2 is diffusion-limited, and a kinetic model was derived.

INTRODUCTION

High-temperature superconductors have demonstrated potential for meeting the technological needs associated with more efficient utilization of electrical distribution grids. In particular, there has been an accelerated effort within the high T_c community on research and development of coated conductors for wire/tape applications [1-7]. These conductors are based on $Ba_2YCu_3O_x$ (Y-213) and $Ba_2RCu_3O_x$ (R=lanthanides) as the principal superconducting materials. They can be deposited on flexible metallic tapes, and the resulting materials show excellent current-carrying capability.

Specially prepared substrates form the basis for coated conductor fabrication. The two state-of-the-art technologies for producing biaxially-textured substrates are commonly known as Ion Beam Assisted Deposition (IBAD) [1-2], and Rolling Assisted Bi-axially Textured Substrate (RABiTS) [3-7]. Typically, the architecture of a RABiTS film includes a number of buffer layers of different materials deposited on a biaxially textured metallic substrate. The general functions of these multilayers are to provide a physical/chemical barrier to substrate oxidation and substrate reaction with the superconductor layer, and to provide texture for crystallographic alignment [8]. Examples of the lower cap layer over the substrate include CeO_2, $SrTiO_3$, Gd_3NbO_7, $LaMnO_3$, and $SrRuO_3$. Often there may be chemical reactions at the interface between $Ba_2YCu_3O_{6+x}$ and the buffer layers, which may partially mitigate the benefits of buffer layers, including the promotion of epitaxial growth of Y-213. Understanding of interfacial reactions of $Ba_2YCu_3O_{6+x}$ with the buffer layers will provide information about how to avoid and/or control the formation of second phases. Phase formation data will further allow better interpretation of the results of TEM analysis of coated conductor interfaces.

We have studied the interfacial reactions of $Ba_2YCu_3O_{6+x}$ with four substrate materials, namely, CeO_2 [9-11], Gd_3NbO_7 [12], $LaMnO_3$ [13], and $SrTiO_3$ [14]. This paper reviews the studies of the multi-component systems representing the interaction of Y-213 with these substrates, particularly the phases formed at the interface. Phase formation and structural studies

of the non-binary systems $Ba_2YCu_3O_{6+x}$-$LaMnO_3$, $Ba_2YCu_3O_{6+x}$-Gd_3NbO_7, $Ba_2YCu_3O_{6+x}$-CeO_2, and $Ba_2YCu_3O_{6+x}$-$SrTiO_3$ were conducted using x-ray diffraction and differential thermal analysis/thermal gravimetric analysis (DTA/TGA).

EXPERIMENTAL[1]

A 10 g master batch of $Ba_2YCu_3O_{6+x}$ was prepared by heating a mixture of BaO, Y_2O_3 and CuO under purified air (CO_2- and H_2O-scrubbed). The BaO starting material was produced from $BaCO_3$ (99.99 % purity, metals basis) by vacuum calcination in a vertical tube furnace. The following heating schedule was used: room temperature to 1300 °C in 20 h; isothermal at 1300 °C for 10 h; 1300 °C to room temperature in 20 h. To prepare $Ba_2YCu_3O_{6+x}$, stoichiometric amounts of BaO, Y_2O_3 and CuO were weighed out in a glove-box, well mixed and calcined in an atmospherically controlled high temperature furnace, first at 850 °C, then at 930 °C repeatedly with intermediate grindings for about two weeks. Ten grams of single-phase master batches of the buffer materials $LaMnO_3$, Gd_3NbO_7, CeO_2, and $SrTiO_3$ were also prepared. The details of the preparation for $LaMnO_3$, Gd_3NbO_7, CeO_2 were described earlier [9-13].

Subsequently, nine samples with different ratios of $Ba_2YCu_3O_{6+x}$ to buffer material were prepared using these master batches of $Ba_2YCu_3O_{6+x}$ and the buffer materials. The ratios prepared were 10:90, 20:80, 30:70, 40:60, 50:50, 60:40, 70:30, 80:20, and 90:10. Pelletized samples were placed inside individual MgO crucibles for annealing in a horizontal box-type controlled-atmosphere furnace. Transfer from the glove-box to the box furnace and vice versa was achieved via a second transfer vessel and an interlock system attached to the furnace. Samples were annealed at 810 °C at p_{O2} = 100 Pa_2, or at 950 °C in purified air repeatedly until no further changes were observed in x-ray diffraction patterns.

X-ray powder diffraction was used to identify the phases synthesized, to confirm phase purity, and to determine phase relationships. A computer-controlled automated Philips diffractometer equipped with a θ-compensation slit and CuK_α radiation was operated at 45 kV and 40 mA. The radiation was detected by a scintillation counter and a solid-state amplifier. All x-ray patterns were measured using a hermetic cell designed for air-sensitive materials [15]. The commercially-supplied Siemens software package and the reference x-ray diffraction patterns of the Powder Diffraction File (PDF) [16] were used for performing phase identification.

Structures of selected member of the product phases were studied using the x-ray Rietveld refinement technique [17]. These samples were mounted as acetone slurries in zero-background quartz holders. A Bruker D8 Advanced Diffractometer equipped with a VANTEC-1 position-sensitive detector was used to measure the powder patterns (CuK_α radiation, 40 kV, 40 mA) [17].

Simultaneous differential thermal analysis and thermogravimetric analysis (DTA/TGA) were used to study thermal events. Most experiments utilized mainly the DTA signal; the TGA signal was useful primarily in following oxygen gain/loss associated with the CuO_x component. DTA/TGA experiments were performed using an electronically upgraded Mettler TA-1 system

[1] Certain commercial equipment, instruments, or materials are identified in this paper in order to specify the experimental procedure adequately. Such identification is not intended to imply recommendation or endorsement by the National Institute of Standards and Technology, nor is it intended to imply that the materials or equipment identified are necessarily the best available for the purpose.

fitted with an Anatech digital control and readout system. The DTA/TGA apparatus was calibrated against the α/β quartz transition (571 °C) and the melting point of NaCl (801 °C), and temperatures reported in this study have a standard uncertainty of ± 5 °C. Event temperatures were determined as the intersection of the baseline with the extrapolated linear portion of the rising DTA peak. Oxygen partial pressure during DTA/TGA was controlled using a previously analyzed Ar/O_2 mixture. During the experiments, gas was continuously flowed through the sample region at a rate of 150 mℓ/min, and the oxygen pressure at the outlet of the DTA/TGA system was periodically checked with a zirconia sensor.

DISCUSSION

The system BYC+ $SrTiO_3$

The study of the interactions of BYC with $SrTiO_3$ have been completed at 810 ºC under 0.1% O_2. We first prepared master batches of BYC and $SrTiO_3$. Then we prepared 9 mixtures with different proportions from these two master batches. From the X-ray study of these 9 samples, we determined the products of reactions. Typical examples of x-ray patterns are shown in Fig. 1. We found that all samples contained $(Ba,Sr)_3YTi_2O_x$, BYC phase, $BaTiO_3$,

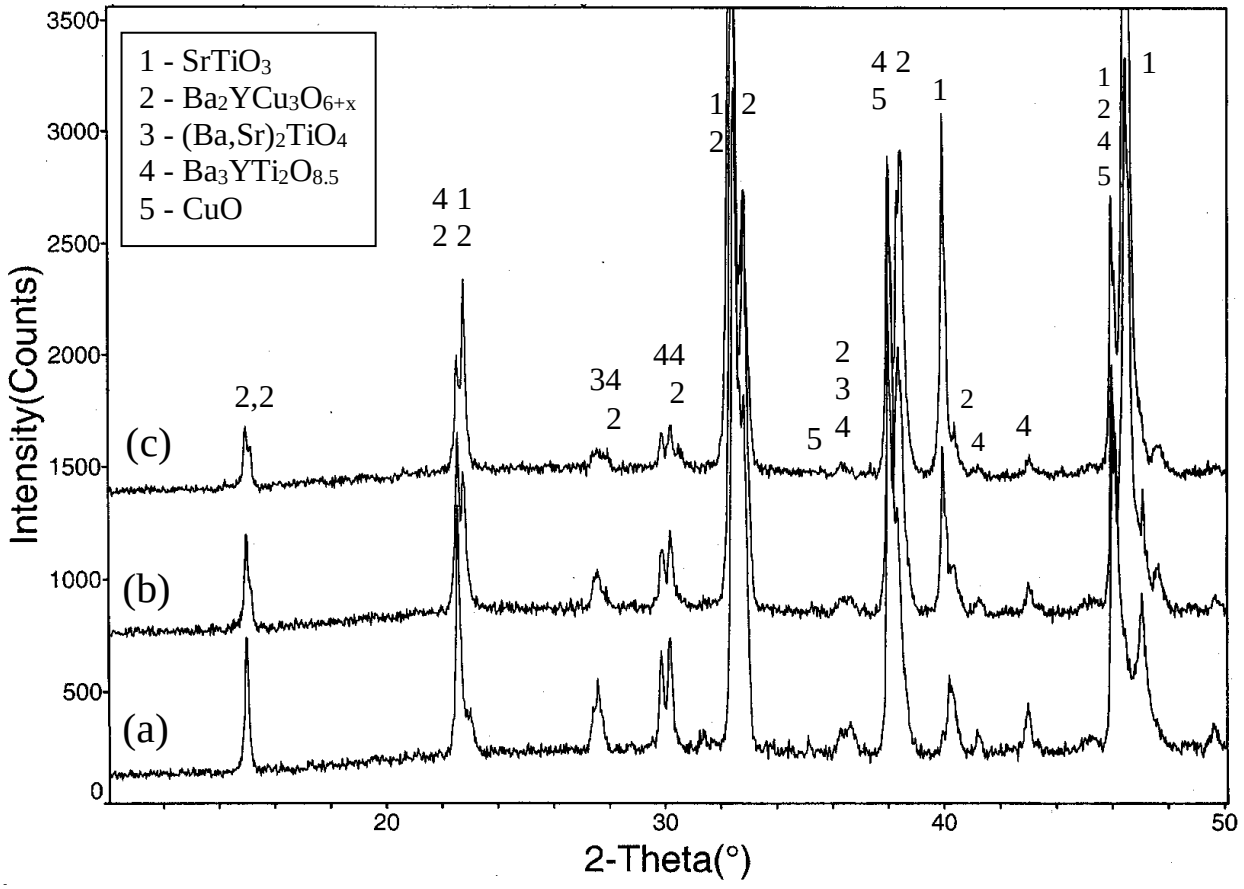

Fig. 1. Typical x-ray patterns showing the presence of small amounts of the phases formed as a result of interaction of $Ba_2YCu_3O_{6+z}$ with $SrTiO_3$ for mixtures with the ratio of (a) 2:8, (b) 6:4, and (c) 8:2. Different amounts of the reaction products are shown as a result of different composition ratios.

Ba_2TiO_4 phase and CuO_x, with different amounts depending on the mixture ratio. The melting temperatures of these compositions ranged from 940 to 970 ºC under 0.1% O_2. Therefore, melting is not likely to be a problem for BYC films on $SrTiO_3$ substrates at processing temperatures below 900 ºC.

Based on a Ba-Sr-Y-Cu-O quaternary diagram that we published earlier, we found that Sr substitutes Ba to a certain degree in a large number of phases in this system. Therefore the phases are written as solid solutions between Ba and Sr. The reactants and products can be represented in the following unbalanced equation:

$$Ba_2YCu_3O_{6+x} + SrTiO_3 \rightarrow (Ba,Sr)_3YTi_2O_x + (Ba,Sr)_2YCu_3O_{6+x} + (Sr,Ba)TiO_3 + (Sr,Ba)_2TiO_4 + CuO_x$$

The 50-50 (Ba,Sr)-BYC solid solution is structurally related to that of the well known BYC phase. We have also studied the crystal chemistry of the lanthanide substituted analogs. The structure of the larger lanthanide compounds (from Pr to Eu) was found to be tetragonal, while that of the smaller size cation compounds are orthorhombic. Convergence of *a* and *b* parameters as a function of ionic radius [18] is demonstrated in Fig. 2.

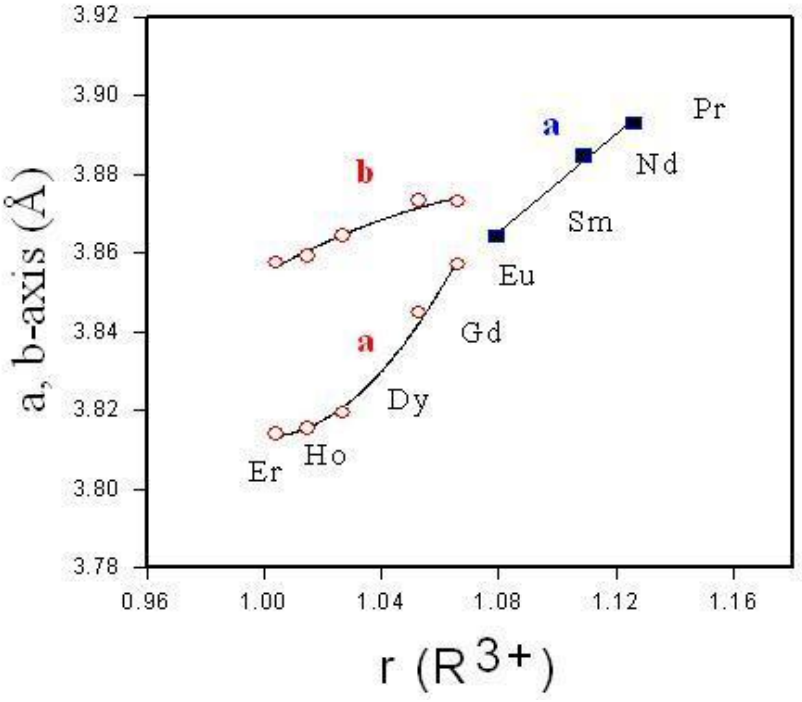

Fig. 2. Plots of a, and b axis of the $(BaSr)_2RCu_3O_{6+x}$ members showing the phase transition from orthorhombic to tetragonal structures between R=Gd and Eu. Convergence of *a* and *b* parameters as a function of ionic radii is demonstrated.

The $(Ba,Sr)_3YTi_2O_x$ phases are hexagonal *P6₃/mmc*. The structure can be considered as related to the 12-layer hexagonal-pervoskite family (Fig. 3). We have also determined the lanthanide series of compounds, $Ba_3RTi_2O_x$ (R=lanthanides). The structure can be viewed as stacking of cubic 'c' and hexagonal 'h' layers (BaO_3) as well as ordered, oxygen deficient pseudocubic c' [BaO_2] layers in the sequence of $(c'cchcc)_2$ along the *c*-axis. The structure units consist of face-sharing TiO_6 octahedral layers, RO_6 layers and TiO_4 tetrahedral layers.

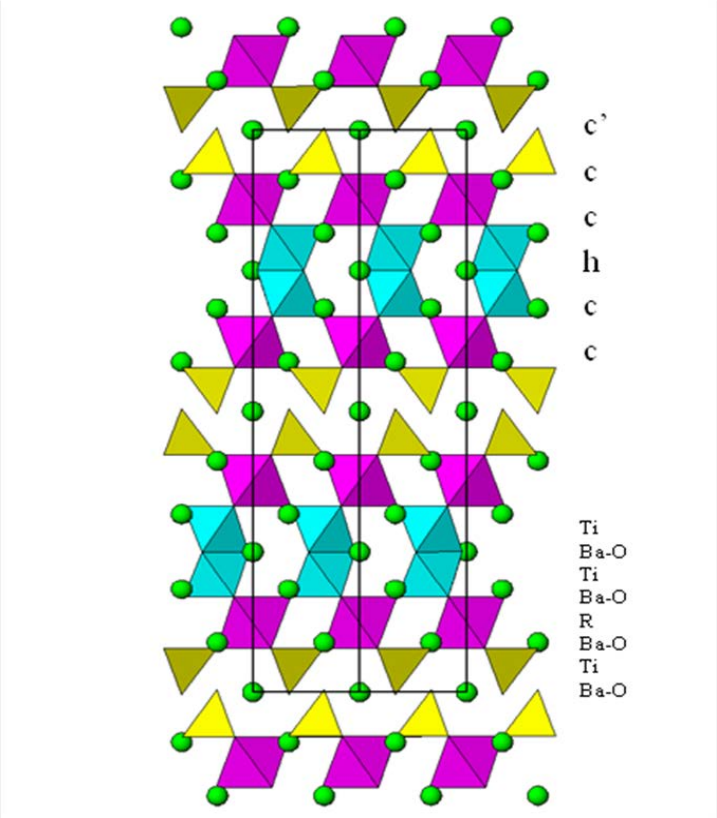

Fig. 3. Perspective view of the $Ba_3RTi_2O_{8.5}$ structure along the [110] direction, showing the stacking of face-sharing TiO_6 octahedral layers, RO_6 layers and TiO_4 tetrahedral layers [18].

The System BYC+ Gd_3NbO_7

X-ray patterns showed that there is a maximum of 5 phases present in each sample. Gd and Y in most cases form solid solutions. DTA temperature of the lowest melting event is around 938 °C in air and 850 °C at 0.1% O_2. Fig 4 gives a representation of the progression of phases from one end to the other, with BYC to Gd_3NbO_7 ratio from 1:9 to 9:1. The compositions can be considered as lying in two 5-phase volumes and a common three-phase boundary (actually a three phase volume due to the presence of solid solutions) between the two five phase volumes.

Compositions on the left of the three-phase boundary consist of the 3 common phases plus $(Y,Gd)_3NbO_7$ and $Ba_2(Gd,Y)NbO_6$; the compositions on the right of the three-phase boundary consist of the 3 common phases plus $Ba_2(Y,Gd)Cu_3O_x$ and the green phase,

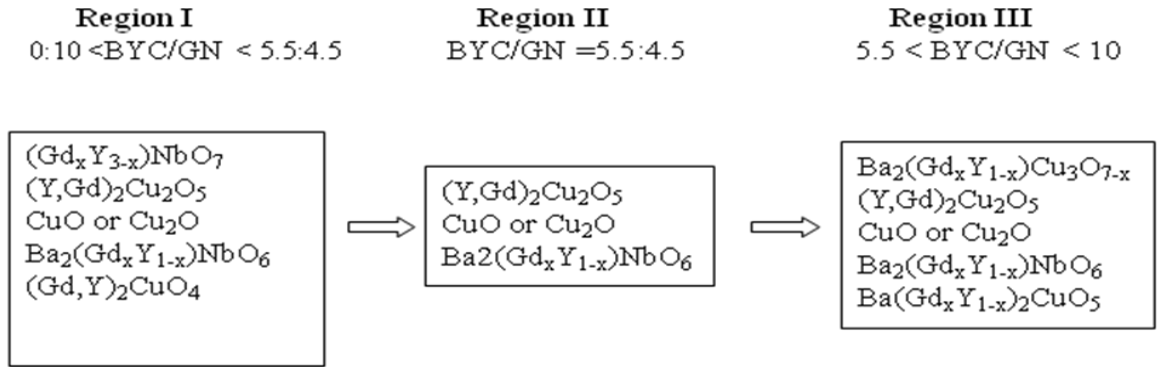

Fig. 4. A schematic representation of three regions of phase assemblages as a function of the compositional ratio of $Ba_2YCu_3O_{6+y}$ (BYC)/Gd_3NbO_7 (GN).

$Ba(Y,Gd)_2CuO_5$. The crossing of the boundary takes place between 5:5 and 6:4 composition ratio between the two end members.

The structure of $(Y,Gd)_3NbO_7$ consists of alternate stacking of distorted NbO_6 octahedra with GdO_8 polygon, forming two dimensional slabs. The additional GdO_7 polyhedra which lie in between these layers are omitted for clarity (Fig. 5). $Ba_2(Gd,Y)NbO_6$ forms a complete solid solution between Gd and Y at high temperature. The NbO_6 octahedra alternates with the $(Gd,Y)O_6$ octahedra in the cubic structure.

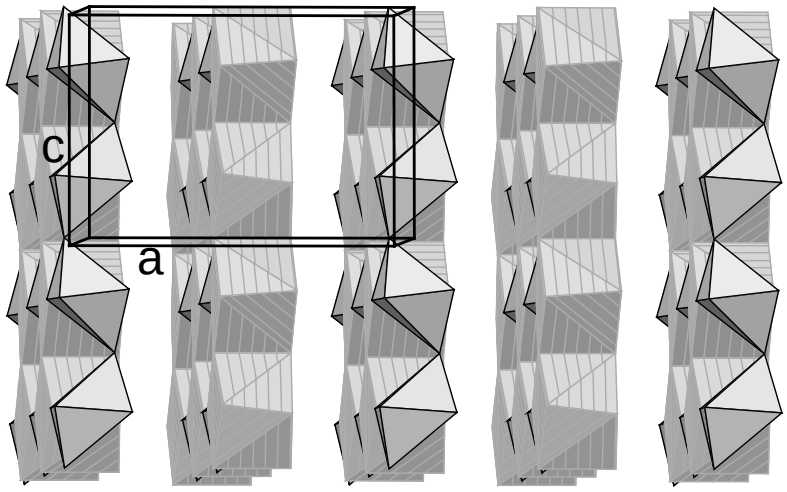

Fig. 5. Crystal structure for Gd_3NbO_7 (*$C222_1$*) showing the partial layered feature. The alternate stacking of distorted NbO_6 octahedra (plain pattern) and $(Gd,Y)O_8$ polyhedra (ruled pattern) are illustrated. The $(Gd,Y)O_7$ polyhedra are omitted for clarity.

The System BYC+ $LaMnO_3$

The interaction between BYC and $LaMnO_3$ have been investigated by determining the phases formed in the non-binary join of the Y213-$LaMnO_3$ system. Based on the x-ray diffraction patterns (Fig. 6) of the 9 samples of different ratios of Y213 and $LaMnO_3$ prepared at 950 °C in purified air and at 810 °C in 100 Pa oxygen, the unbalanced equation representing the chemical reactions can be written as:

$$Ba_2YCu_3O_{6+z}+LaMnO_3 \rightarrow Ba_{2-x}(La_{1+x-y}Y_y)Cu_3O_{6+z}+Ba(Y,La)_2CuO_5+(La,Y)MnO_3+(La,Y)Mn_2O_5$$

In this equation, general formulas which are written with '(La, Y) or (Y, La)' are used to represent possible solid solution formation between La, and Y. We found that La and Y indeed form solid solution in the $Ba(Y,La)_2CuO_5$ phase to a small extent in air and in 0.1% O_2. But there is no evidence of solid solution formation in the $(La,Y)Mn_2O_5$ phase under the present synthesis conditions. The structure of the $LaMn_2O_5$ phase consists of infinite chains of $Mn^{4+}O_6$ edge-sharing octahedra, linked by $Mn^{3+}O_5$ and YO_6 units. The Mn ions adopt 3+ and 4+ valence states.

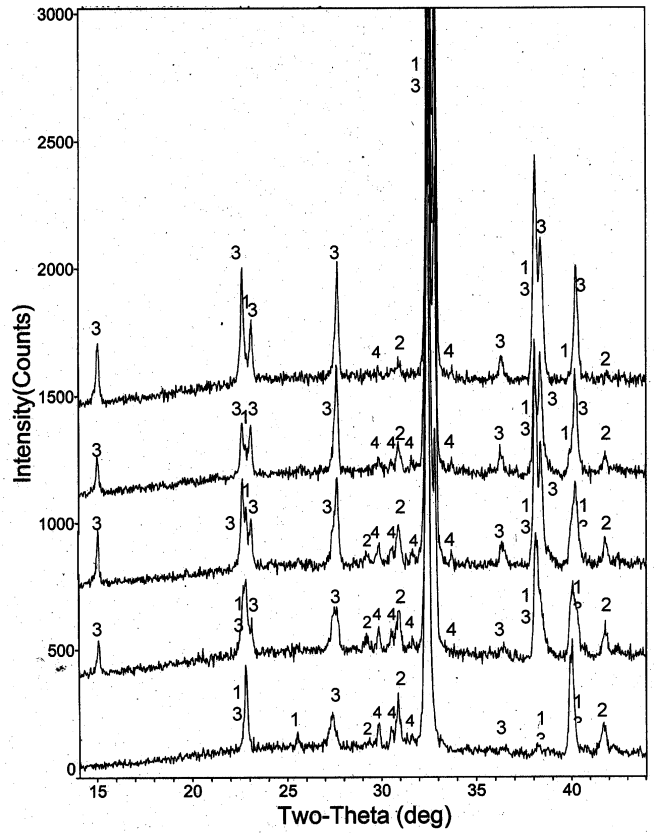

Fig. 6. XRD patterns representing the reaction of $Ba_2YCu_3O_{6+z}$ with $LaMnO_3$ in different mole ratios of 10:90, 30:70, 50:50, 70:30, and 90:10 (810 ºC, p_{O2} = 100 Pa). The labeling in the figure is as follows: 1- (La,Y)MnO_3, 2-(La,Y)Mn_2O_5, 3- $Ba_{2-x}(La_{1+x-y}Y_y)Cu_3O_{6+z}$, 4-$Ba(Y,La)_2CuO_5$.

The System BYC+CeO_2

Since CeO_2 is an important buffer material, we have conducted more detailed work on this system. We described their interactions in terms of both phase equilibria and kinetics. The equilibria along the $Ba_2YCu_3O_{6+x}$-CeO_2 non-binary join are shown in the context of the BaO-Y_2O_3-CuO_x-CeO_2 framework in Fig. 7. This join passes through two 4-phase regions, namely: $Ba_2YCu_3O_{6+x}$-$BaCeO_3$-BaY_2CuO_5-Cu_2O and $BaCeO_3$-BaY_2CuO_5-Cu_2O-CeO_2. These two volumes are mutually consistent. These two tetrahedra share a common plane defined by BaY_2CuO_5, Cu_2O and $BaCeO_3$. The green phase and $BaCeO_3$ are part of the products of reaction. As a composition vector passes through the two tetrahedra, only three phases are observed at the boundary. This phase boundary exists at the mole ratio of $Ba_2YCu_3O_{6+x}$: CeO_2 = 40 : 60. Cerium is known to possess various oxidation states. Under the present conditions, CeO_2 is the stable form.

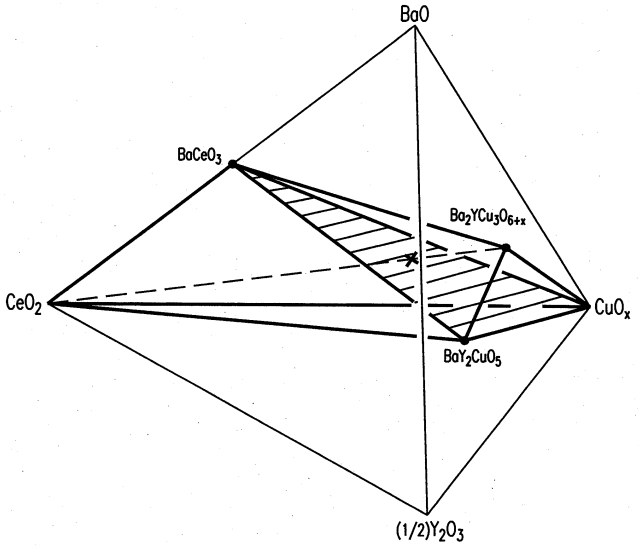

Fig. 7. The BaO-Y_2O_3-CuO_x-CeO_2 tetrahedron showing the two sub-volumes $Ba_2YCu_3O_{6+x}$ - $Ba(Ce,Y)O_{3-x}$ - BaY_2CuO_5 - Cu_2O and $BaCeO_3$-BaY_2CuO_5- Cu_2O-CeO_2, within which the compositions of the $Ba_2YCu_3O_{6+x}$-CeO_2 join lie. "$BaCeO_3$" is a solid solution with the formula $Ba(Ce_{1-z}Y_z)O_{3-x}$. The "x" indicates the intersection of the $Ba_2YCu_3O_{6+x}$-CeO_2 join with the $BaCeO_3$ – BaY_2CuO_5 - CuO_x plane.

We conducted a preliminary study to obtain the appropriate temperature range for heat treatments: 790 °C, 810 °C, and 830 °C. For each sample, each subsequent heat treatment was in general doubled in time. X-ray diffraction was used to obtain intensity of selected reflections of these samples. For example, we used the (031) reflection for Y213, (213) reflection for $BaCeO_3$, and (131) reflection for the green phase. The intensity values are assumed to be proportional to

the amount of a particular phase, or the thickness of the reaction layer. TEM study was carried out to obtain the microstructure, including the thickness of the reaction layer. A kinetics model was then derived to understand the progress of reaction.

The x-ray patterns of the sample heat-treated at 810 °C at various times is shown in Fig. 8. The development of peaks related to $Ba(Ce,Y)O_3$, the green phase and CuO phases are shown. As the amount of reaction time increases, we clearly see the decrease of the peak intensity of the reactant BYC phase, the increase of intensity of the products $Ba(Ce,Y)O_3$ phase and the green phase, BaY_2CuO_5.

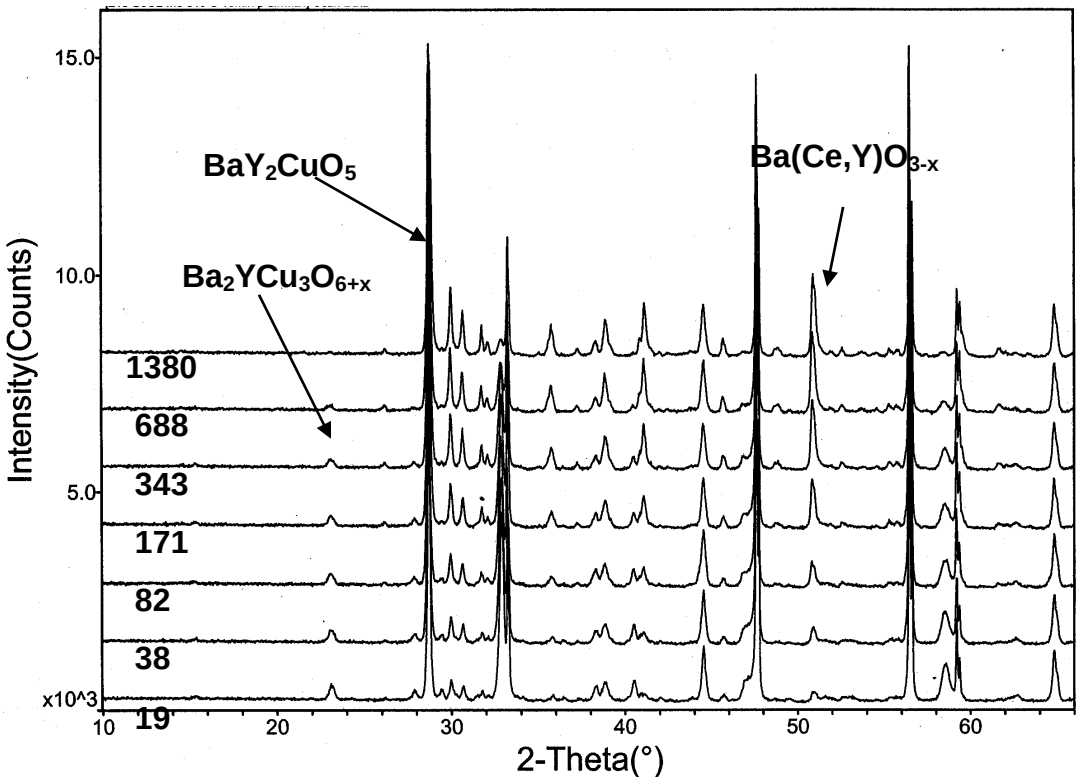

Fig. 8. Sequential x-ray diffraction patterns of $Ba_2YCu_3O_{6+x}/CeO_2$ pellet heat-treated at 810 °C for increasing cumulative time (minutes).

To study the kinetics of reaction, we deposited BYC films on CeO_2 pellets using our NIST laser deposition facility. The optical images of the CeO_2 pellet on the left, and the one with BYC deposited on the right (Fig. 9). The diameter of the pellets is about 10 mm. They both have smooth surfaces. In most ceramic reactions such as this, there is a reaction interface between reacting phases. The overall process involves transport of material to the interface, reaction at the interface, and sometimes transport of reaction products away from the interface [19]. For a reaction in which a compound is formed as the *planar* reaction layer, and the rate of product formation is controlled by diffusion through the product layer, then the reaction kinetics obey the

parabolic rate rule, $x = Kt^{1/2}$ (where x is thickness of the reaction layer, *t* is time, and K is a constant related to the rate constant).

We indeed found in all samples studied, that a parabolic rate law is obeyed. The plots of intensity vs. $t^{1/2}$ for the experiments at 810 °C are shown in Fig. 10. For the products $Ba(Ce,Y)O_3$ and green phase, the shape of the curves are found to be rather similar. There is the straight-line portion of these curves at a relatively short reaction time period, and then the change of intensity decreases. While the intensity of product increases, that of the reactant, namely the BYC, decreases. The intensity vs. $t^{1/2}$ plots for the experiments at 830 °C are similar to those of

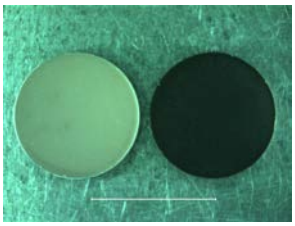

Fig. 9. Optical images of uncoated CeO_2 (left) and $Ba_2YCu_3O_{6+x}/CeO_2$ (right) (scale indicator = 10 mm).

810 °C. A linear portion of the curves for the products at short reaction times is found, and then the slope becomes flat. If we compare the phase formation feature of $Ba(Ce,Y)O_3$ at the three different temperatures (Fig. 11), we observe that at higher temperature, 830 °C, the formation of $Ba(Ce,Y)O_3$ was completed earlier, i.e. the reaction progressed faster, as expected. The reaction to form $Ba(Ce,Y)O_3$ was nearly complete at $t^{1/2}$ of about 13.5 $min^{1/2}$. At 810 °C the corresponding time parameter was longer at $t^{1/2}$ = 23 $min^{1/2}$. At 790 °C, the reaction was still occurring at $t^{1/2}$ = 60 $min^{1/2}$.

The bright-field image of a cross-section of a sample heat-treated at 830 °C for 123 minutes was used to obtain the thickness of the reaction layer of reaction. Electron energy loss spectroscopy/energy dispersive spectroscopy (EELS/EDS) measurements in TEM confirmed existence of a monophasic reaction layer about 0.4 μm thick, comprised of $Ba(Ce,Y)O_{3-x}$. A mixture of BYC, green phase, and CuO was also observed in the immediate vicinity of $Ba(Ce_{1-z}Y_z)O_{3-x}$, whereas the outer part of the film consisted primarily of unreacted Y-213. Using a thickness of 0.40 μm, the parabolic equation gives a value of 4.7 x 10^{-3} $\mu m/s^{1/2}$ for K at 830 ºC. The activation energy for the reaction was derived using the Arrhenius Equation [20]:

$$K_1/K_2 = [Ae^{(-Eact/RT_1)}/Ae^{(-Eact/RT_2)}] \qquad (1)$$

where K_1 and K_2 are constants relating to the reaction rate at temperatures T_1 and T_2 (Kelvin), respectively. A is an empirical pre-exponential factor, E_{act} is the activation energy, and R is the gas constant. K_1 and K_2 were obtained from the parabolic law $x = Kt^{1/2}$, as discussed above. From the experiments at 790 ºC (1063 K) and 830 ºC (1103 K), K_1 = 0.0016 $\mu m/s^{1/2}$ and K_2 = 0.0047 $\mu m/s^{1/2}$, and E_{act} = 2.67 x 10^5 J/mol. This activation energy is similar in magnitude to activation energies reported for reactions between other multicomponent ceramic oxides [21,

22]. The fact that a monophasic product layer of $Ba(Ce_{1-z}Y_z)O_{3-x}$ was formed adjacent to the CeO_2 suggests that the reaction occurred primarily by diffusion of Ba into the CeO_2. This process left behind products of green phase and CuO.

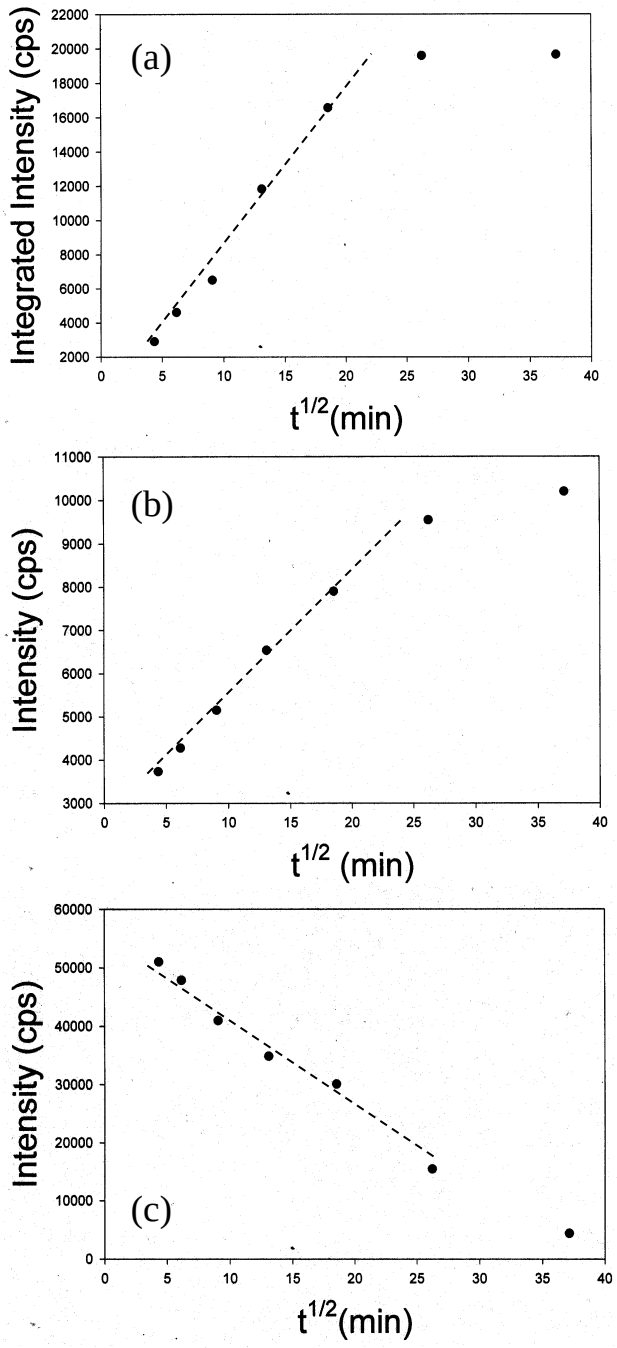

Fig. 10. Plots of integrated intensity vs. cumulative (time, minutes)$^{1/2}$ (a) $Ba(Ce_{1-z}Y_z)O_{3-x}$, (reflection 213), (b)BaY_2CuO_5 (reflection 131), and (c) $Ba_2YCu_3O_{6+x}$ (reflection 031) for samples heat-treated at 810 °C. 'cps' indicates counts per second.

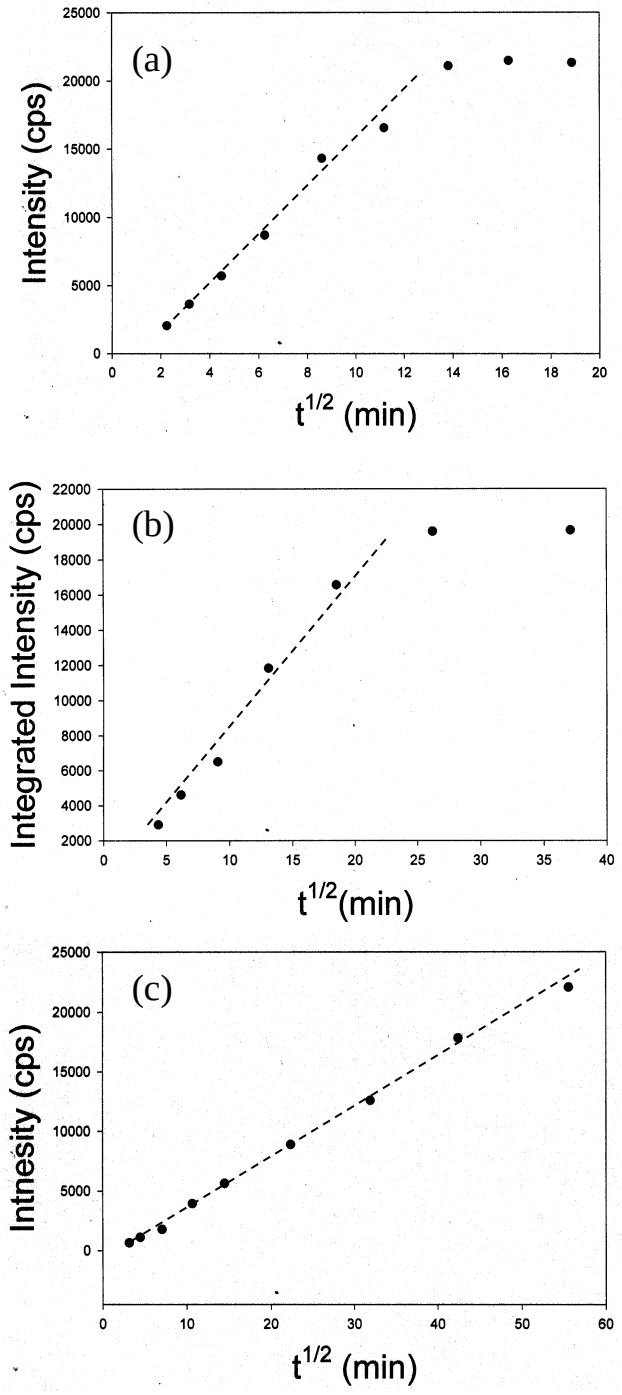

Fig. 11. Plots of integrated intensity vs. cumulative (time, minutes)$^{1/2}$ of $Ba(Ce_{1-z}Y_z)O_{3-x}$ (reflection 213) at three different temperatures, (a) 830 °C, (b) 810 °C, and (c) 790 °C. 'cps' indicates counts per second.

SUMMARY

As a summary, we have studied the reactions of BYC with $SrTiO_3$, Gd_3NbO_7, and $LaMnO_3$ in terms of crystal chemistry and crystallography of the phases formed. With CeO_2 we also studied kinetics of reactions. The reaction falls in two 4-phase fields. We followed the kinetics of reaction by monitoring the product phases $Ba(Ce_{1-z}Y_z)O_{3-x}$ and BaY_2CuO_5 as a function of time and temperature. The reaction kinetics obey a simple parabolic rate law, characteristic of diffusion-limited processes. The $Ba_2YCu_3O_{6+x}$ /CeO_2 reaction is limited by solid-state diffusion, and the reaction kinetics obey the parabolic rule, $x = Kt^{1/2}$ (where x is thickness of the reaction layer, *t* is time, and K is a constant related to the rate constant); K was determined to be 1.6 x 10^{-3} $\mu m/s^{1/2}$ at 790 ºC and 4.7 x 10^{-3} $\mu m/s^{1/2}$ at 830 ºC. The activation energy for the reaction was determined to be E_{act} = 2.67 x 10^5 J/mol using the Arrhenius Equation.

REFERENCES

[1] P. N. Arendt, S.R. Foltyn, L. Civale, R.F. DePaula, P.C. Dowden, J.R. Groves, T.G. Holesinger, Q.X. Jia, S. Kreiskott, L. Stan, I. Usov, H. Wang, and J.Y. Coulter, *Physica C* 412-414 (2004) 795-800.

[2] S. R. Foltyn, E.J. Peterson, J.Y. Coulter, P.N. Arendt, Q.X. Jia, P.C. Dowden, M.P. Maley, X.D. Wu, D.E. Peterson, *J. Mater. Res.* 12 (1997) 2941-2946.

[3] A.P. Malozemoff, S. Annavarapu, L. Fritzemeier, Q. Li, V. Prunier, M. Rupich, C. Thieme, W. Zhang, A. Goyal A., Paranthaman M., and Lee D.F., Supercond. Sci. Technol. **13** 473-476 (2000).

[4] M. Paranthaman, C. Park, X. Cui, A. Goyal, D.F. Lee, P.M. Martin, T.G. Chirayil, D.T. Verebelyi, D.P. Norton, D.K. Christen, and D.M. Kroeger, J. Mater. Res **15** (12) 2647-2652 (2000).

[5] A. Goyal, D.F. Le, F.A. List, E.D. Specht, R. Feenstra, M. Paranthaman, X. Cui, S.W. Lu, P.M. Martin, D.M. Kroeger, D.K. Christen, B.W. Kang, D.P. Norton, C. Park, D.T. Verebelyi, J.R. Thompson, R.K. Williams, T. Aytug, and C. Cantoni, Physica C **357** 903-913 (2001).

[6] T. Aytug, A. Goyal, N. Rutter, M. Paranthaman, J.R. Thompson, H.Y. Zhai, and D.K. Christen, J. Mater. Res. **18** [4] 872-877 (2003).

[7] M. Paranthaman, A. Goyal, F.A. List, E.D. Specht, D.F. Lee, P.M. Martin, Q. He, D.K. Christen, D.P. Norton, J.D. Budai, D.M. Kroeger, Physica C **275** 266-272 (1997).

[8] M. Rupich, American Superconductor Corporation, Devens, MA 01434, private communication.

[9] W. Wong-Ng, L.P. Cook, P. Schenck, I. Levin, Z. Yang, Q. Huang, and J. Frank, Proceedings of the PACRIM meeting, sponsored by ACerS, Maui, Hawaii, September, 2005; Ceramic Transactions series **191** 83-98 (2006).

[10] W. Wong-Ng, Z. Yang, L.P. Cook, Q. Huang, and J. Frank, "Chemical Interaction Between $Ba_2YCu_3O_{6+x}$ and CeO_2 at p_{O2} = 100 Pa," Solid States Sci, **7** 1333-1343 (2005).

[11] L. P. Cook, W. Wong-Ng, P. Schenck, Z. Yang, I. Levin, and J. Frank, "Kinetics Studies of the Interfacial Reactions of the $Ba_2YCu_3O_{6+x}$ Superconductor with CeO_2 Buffer Systems," J. Electronic Mater. **36**(10), 1293-1298 (2007)

[12] W. Wong-Ng, Z. Yang, J. A. Kaduk, L.P. Cook, and M. Paranthaman, ", J. Solid State Chem. **470**(5-6) 345-351 (2010).

[13] G. Liu, W. Wong-Ng, J. A. Kaduk, and L.P. Cook, "Interactions of $Ba_2YCu_3O_{6+y}$ with Substrate Layer $LaMnO_3$ in Coated Conductors", Physica C, **470** (5-6) 341-351 (2010).
[14] W. Wong-Ng, Y. Zhi, J. A. Kaduk, L. P. Cook, S. Diwanji, and C. Lucas, "Interactions of $Ba_2YCu_3O_{6+x}$ with $SrTiO_3$ Substrate," to be submitted to J. Solid State Chem. (2010).
[15] Ritter J.J., Powd. Diffr. **3** 30-31 (1988).
[16] PDF, Powder Diffraction File, produced by International Centre for Diffraction Data, 12 Campus Blvd., Newtown Squares, PA. 19073-3273, USA.
[17] Larson, A.C., von Dreele, R.B., *General Structure Analysis System (GSAS)*, Los Alamos National Laboratory Report LAUR 86-748, Los Alamos, USA (2004).
[18] R.D. Shannon, Acta Crystallogr. **A32**, 751-767 (1976).
[19] Kingery W.D., Bowen H.K., and Uhlmann D.R., *Introduction to Ceramics*, 2nd Ed., pp. 381-447, John Wiley & Sons, New York, USA, 1976.
[20] Laidler, K. J., *Chemical Kinetics*,Third Edition, Benjamin-Cummings, (1997).
[21] Shiue J-T. and Fang T-T., J. Mater. Res. 18(11) 2594-2599 (2003).
[22] Xu J., Zhu X. H. and Meng Z. V., IEEE Trans. Components and Packaging Technol. 22(1) 11-16 (1999).